

# Theoretical investigation of efficiency of a p-a-SiC:H/i-a-Si:H/n- $\mu$ c-Si solar cell\*

Deng Qingwen(邓庆文)<sup>1,†</sup>, Wang Xiaoliang(王晓亮)<sup>1,2</sup>, Xiao Hongling(肖红领)<sup>1,2</sup>, Ma Zeyu(马泽宇)<sup>1</sup>, Zhang Xiaobin(张小宾)<sup>1</sup>, Hou Qifeng(侯奇峰)<sup>1</sup>, Li Jinmin(李晋闽)<sup>1</sup>, and Wang Zhanguo(王占国)<sup>2</sup>

(1 Materials Science Center, Institute of Semiconductors, Chinese Academy of Sciences, Beijing 100083, China)

(2 Key Laboratory of Semiconductor Materials Science, Institute of Semiconductors, Chinese Academy of Sciences, Beijing 100083, China)

**Abstract:** A solar cell with a novel structure is investigated by means of the analysis of microelectronic and photonic structure (AMPS). The power conversion efficiency is investigated with the variations in interface recombination velocity, thicknesses of p-type layer, intrinsic layer, n-type layer, and doping density. Results show that it is available and preferable in theory to employ a-SiC:H as a window layer in p-a-SiC:H/i-a-Si:H/n- $\mu$ c-Si solar cells, and provide a new approach to improving the power conversion efficiency of amorphous silicon solar cells.

**Key words:** solar cell; simulation; efficiency; AMPS

**DOI:** 10.1088/1674-4926/31/10/103003

**PACC:** 8630J; 6185

## 1. Introduction

Silicon solar cells have been investigated for many years. In particular, amorphous silicon (a-Si) has been favored for its better characteristics compared to crystalline silicon and polysilicon, such as higher absorption coefficient, better response in low light environment and lower cost. Nevertheless, the Staebler–Wronski effect (S–W effect) of amorphous silicon reduces the conversion efficiency. In order to reduce the light-induced degradation connected with the porosity of the intrinsic layer of hydrogenated amorphous silicon (a-Si:H)<sup>[1]</sup>, Chowdhury *et al.*<sup>[2]</sup> have implemented smaller grain size (less than 3 nm diameter) and intermediate range order to provide better stability in the intrinsic layer near the p-type/intrinsic (p/i) interface, and they have achieved the minimum degradation efficiency of 2%. A novel structure of a-Si:H solar cell has been designed by two-dimensional device simulation<sup>[3]</sup>, and the results show that the quantum efficiency has been improved. Ulyashin *et al.*<sup>[4]</sup> have designed heterojunction solar cells with the structure of Indium Tin Oxide/n-type a-Si:H/p-type crystalline silicon (ITO/(n)a-Si:H/(p)c-Si). They have investigated the impact on conversion efficiency of deposition temperature, and have concluded that the interface modification of the solar cell has a more significant impact on the quality of the heterojunction solar cells than that of the a-Si:H layer. Murthy *et al.*<sup>[5]</sup> have investigated the defect states in bulk of the intrinsic layer and at the p-type/intrinsic (p<sup>+</sup>/i) interface using dark reverse current-voltage measurements, and the results show that simulated and measured reverse leakage current characteristics are in reasonable agreement. Yang *et al.*<sup>[6]</sup> have implemented the structure of hydrogenated amorphous silicon/hydrogenated amorphous silicon germanium/hydrogenated nanocrystalline silicon

(a-Si:H/a-SiGe:H/nc-Si:H) and achieved an initial active area efficiency of 14.6%.

Compared to crystalline silicon single junction solar cells, microcrystalline silicon ( $\mu$ c-Si) single junction solar cells have worse reliability<sup>[7]</sup> and lower efficiency<sup>[8]</sup> for the existence of grain boundaries and defects which degrade the optical and electric properties. Traditionally,  $\mu$ c-Si is usually employed as one part in a heterojunction solar cell so as to lessen these negative effects.

The analysis of microelectronic and photonic structure (AMPS) program has been utilized to analyze the characteristics of photovoltaic devices by simulations<sup>[9–12]</sup>. However, most of the window layer materials are a-Si:H and  $\mu$ c-Si in silicon tandem solar cells. In this work, hydrogenated amorphous silicon carbide (a-SiC:H) is employed as a window layer. For one thing, the optical gap in p-doped a-SiC:H changes from 1.7 to 2.0 eV with the variation in doping density, which is wider than that of crystalline silicon and amorphous silicon. For another thing, a-SiC:H films provide a wide range of electrical conductivity without a drastic change in the optical gap<sup>[13]</sup>. The a-Si:H, whose response in low light environment and absorption coefficient are excellent, suits the light absorption layer material. Therefore, a novel structure with p-a-SiC:H/i-a-Si:H/n- $\mu$ c-Si is utilized. To the best of our knowledge, this structure is firstly investigated in theory, though a-Si:H has been investigated for many years.

## 2. Models and simulations

### 2.1. DOS model

The density of states (DOS) model<sup>[14]</sup> is utilized in this work. The schematic of a p-a-SiC:H/i-a-Si:H/n- $\mu$ c-Si solar cell is shown in Fig. 1(a), and the energy band diagram is shown

\* Project supported by the Knowledge Innovation Engineering of the Chinese Academy of Sciences (No. YYYJ-0701-02), the National Natural Science Foundation of China (Nos. 60890193, 60906006), the State Key Development Program for Basic Research of China (Nos. 2006CB604905, 2010CB327503), and the Knowledge Innovation Program of the Chinese Academy of Sciences (Nos. IS-CAS2008T01, ISCAS2009L01, ISCAS2009L02).

† Corresponding author. Email: daven@semi.ac.cn

Received 15 March 2010, revised manuscript received 24 May 2010

© 2010 Chinese Institute of Electronics

Table 1. Parameters for simulations.

Parameters, e, h for electrons and holes, respectively	p-a-SiC:H	i-a-Si:H	n- $\mu$ c-Si
Electron affinity (eV)	3.7	3.8	3.8
Mobility band gap (eV)	1.92	1.82	1.3–1.6
Optical band gap (eV)	1.88	1.72	1.7
Relative dielectric constant	11.9	11.9	11.9
Effective conduction band density ( $\text{cm}^{-3}$ )	$2.5 \times 10^{20}$	$2.5 \times 10^{20}$	$3 \times 10^{19}$
Effective valence band density ( $\text{cm}^{-3}$ )	$2.5 \times 10^{20}$	$2.5 \times 10^{20}$	$2 \times 10^{19}$
Electron mobility ( $\text{cm}^2/(\text{V}\cdot\text{s})$ )	10	20	40
Hole mobility ( $\text{cm}^2/(\text{V}\cdot\text{s})$ )	1	2	4
Band tail density of states ( $\text{cm}^{-3}\cdot\text{eV}^{-1}$ )	$1 \times 10^{21}$	$1 \times 10^{21}$	$2 \times 10^{20}$
Characteristic energy (eV) donors, acceptors, respectively	0.1, 0.05	0.05, 0.02	0.01, 0.01
Capture cross section for donor states, e, h, ( $\text{cm}^2$ )	$10^{-17}, 10^{-15}$	$10^{-17}, 10^{-15}$	$10^{-17}, 10^{-15}$
Capture cross section for acceptor states, e, h, ( $\text{cm}^2$ )	$10^{-17}, 10^{-15}$	$10^{-17}, 10^{-15}$	$10^{-17}, 10^{-15}$
Gaussian density of states ( $\text{cm}^{-3}$ )	$1 \times 10^{16}$	$5 \times 10^{15}$	—
Gaussian peak energy (eV) donors, acceptors, respectively	1.17, 1.27	1.02, 1.12	—
Standard deviation (eV)	0.08	0.08	—
Capture cross section for donor states, e, h, ( $\text{cm}^2$ )	$10^{-14}, 10^{-15}$	$10^{-14}, 10^{-15}$	—
Capture cross section for acceptor states, e, h, ( $\text{cm}^2$ )	$10^{-15}, 10^{-14}$	$10^{-15}, 10^{-14}$	—
Switch-over energy measured positively from valence band (eV)	—	—	0.56
Density of acceptor-like and donor-like midgap states ( $\text{cm}^{-3}\cdot\text{eV}^{-1}$ )	—	—	$10^{15}$
Capture cross section in donor midgap states, e, h ( $\text{cm}^2$ )	—	—	$10^{-14}, 10^{-16}$
Capture cross section in acceptor midgap states, e, h ( $\text{cm}^2$ )	—	—	$10^{-16}, 10^{-14}$

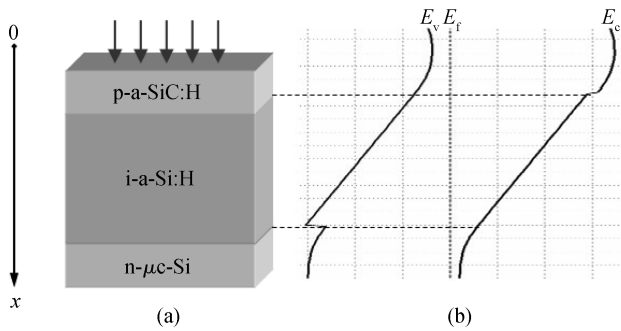


Fig. 1. Diagrams of a p-a-SiC:H/i-a-Si:H/n- $\mu$ c-Si solar cell. (a) Skeleton drawing. (b) Energy band diagram. Conduction band ( $E_c$ ), Fermi level ( $E_f$ ), valence band ( $E_v$ ).

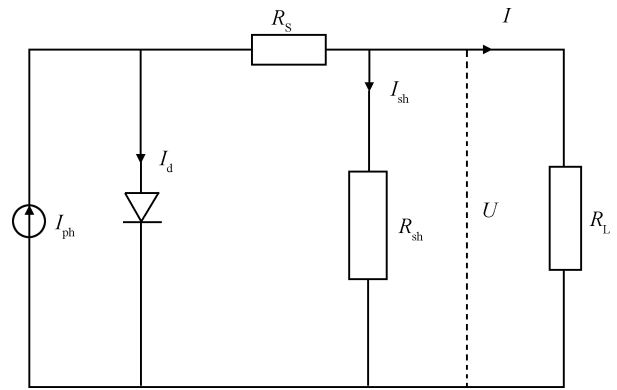


Fig. 2. Equivalent circuit diagram based on diode model: the photo-induced current ( $I_{ph}$ ), the diode current ( $I_d$ ), the shunt resistance ( $R_{sh}$ ) current ( $I_{sh}$ ), the series resistance ( $R_s$ ), the load resistance ( $R_L$ ), and the output voltage ( $U$ ).

in Fig. 1(b). The default thicknesses of the p-type layer, intrinsic layer and n-type layer are 30, 500 and 35 nm, respectively, and the default doping densities of donor and acceptor are  $10^{19}$  and  $10^{18} \text{ cm}^{-3}$ , respectively. The default reflection coefficients at the front interface (p-a-SiC:H/i-a-Si:H interface, RF for short) and the back interface (i-a-Si:H/n- $\mu$ c-Si interface, RB for short) are 0.1 and 0.9, respectively, and the default interface recombination velocities are  $10^7 \text{ cm/s}$ . The interface recombination velocities for electrons and holes at the p-a-SiC:H/i-a-Si:H interface, SNO and SPO for short, respectively. The interface recombination velocities for electrons and holes at the i-a-Si:H/n- $\mu$ c-Si interface, SNL and SPL for short, respectively.

## 2.2. Diode model

In this work, a diode model is implemented to investigate the circuit characteristics of p-SiC/i-a-Si:H/n- $\mu$ c-Si solar cells. The equivalent circuit diagram is shown in Fig. 2.

The current  $I$  is given by

$$I = I_{ph} - I_0 \left[ \exp \left( q \frac{U + IR_s}{kT} \right) - 1 \right] - \frac{U}{R_{sh}}, \quad (1)$$

where  $I_0$  is the reverse saturation current,  $k$  is Boltzmann constant,  $q$  is the electron charge, and  $T$  is the temperature.

## 2.3. Simulation

The efficiency is discussed by simulations, and most parameters<sup>[15]</sup> are shown in Table 1. All results are achieved at AM 1.5 illumination and 300 K.

# 3. Results and discussions

## 3.1. Interface recombination

Interface recombination is one of the important recombination models. Different interface recombination velocities are

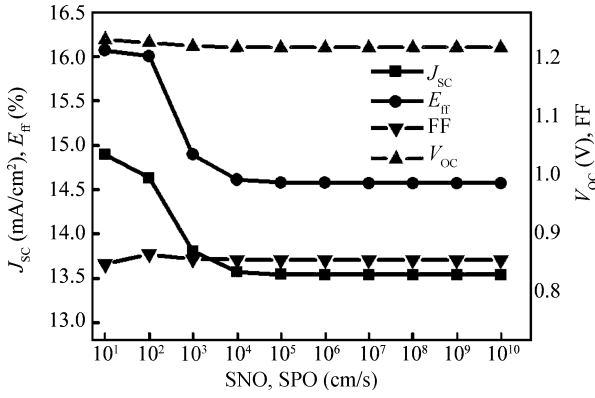


Fig. 3. Impacts on  $V_{oc}$ ,  $J_{sc}$ , FF and  $E_{ff}$  come from interface recombination velocity.

applied to investigate the impacts on short-circuit current density ( $J_{sc}$ ), open-circuit voltage ( $V_{oc}$ ), fill factor (FF) and efficiency ( $E_{ff}$ ). The results are shown in Fig. 3, which is completed with the neglects of interface recombination, band tail states, and band gap defects. In this simulation, the  $R_s$  mainly depends on the material properties, such as the interface recombination velocity, and whether the defects exist or not. Assume that the square of this solar cell is unity square centimeter.

From Fig. 3, it can be seen that  $J_{sc}$  and  $E_{ff}$  drastically decline in the range where SNO and SPO are less than  $10^4$  cm/s. The reason is that the increase in interface recombination velocity reduces the number of holes and electrons collected by the electrodes so that the short-circuit current reduces. The efficiency can be expressed as

$$E_{ff} = \frac{J_{sc} V_{oc} FF}{P_{in}}, \quad (2)$$

where  $P_{in}$  is the incident power per unit area.

According to Eq. (1), one can see that  $E_{ff}$  declines with the drop in  $J_{sc}$  when  $V_{oc}$  and FF nearly remain stable. In light of the results of the simulation from AMPS and Eq. (1),  $R_s$  and  $R_{sh}$  are calculated ( $\sim 1.25 \Omega$  and  $\sim 20000 \Omega$ , respectively, when  $SNO = SPO = 1000$  cm/s). The other values of  $R_s$  and  $R_{sh}$  related to SPO and SNO can also be calculated with the same method. Experimentally, the SNO, SPO, SNL and SPL should be controlled into small values by optimizing the conditions of material growth in order to improve the power conversion efficiency.

### 3.2. Band tail states and band gap states

Band tail states include band tail state density, donor characteristic energy and acceptor characteristic energy, and capture cross section for donor states and acceptor states including electrons and holes, respectively.

Band gap states include Gaussian defect states and flat distribution states. Gaussian defect states require Gaussian density of states, Gaussian peak energy for donors and acceptors, standard deviation and capture cross section for donor states and acceptor states. Flat distribution states require switch-over energy measured positively from valence band, density of acceptor-like and donor-like midgap states, and capture cross section in donor midgap states and acceptor midgap for electrons and holes, respectively.

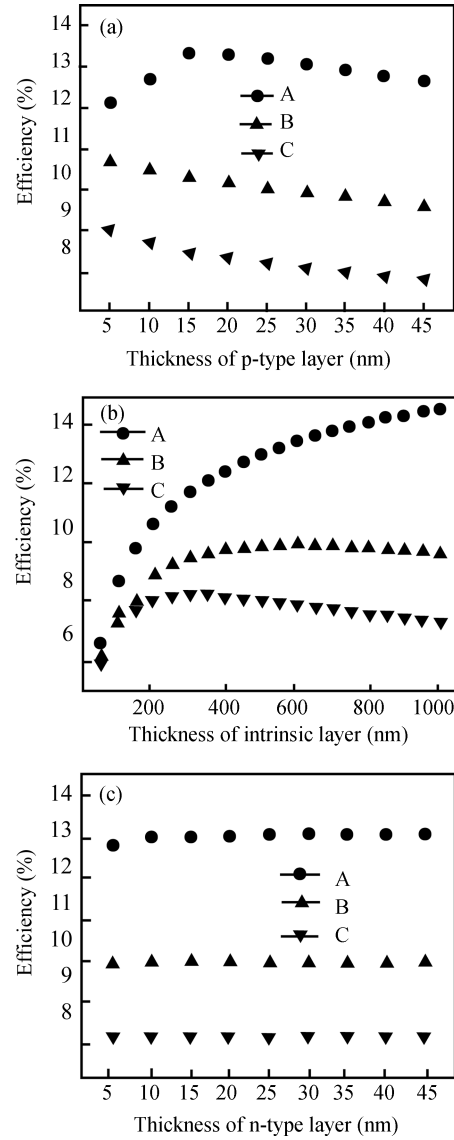


Fig. 4. Impacts on efficiency come from the thickness of each layer. (a) p-type layer. (b) Intrinsic layer. (c) n-type layer. A, B and C indicate the conditions without band tail states and band gap states, with band tail states but without band gap states, with band tail states and band gap states in each layer, respectively.

From Fig. 4, it can be seen that the thicknesses of the p-type layer and the intrinsic layer has more significant impact on efficiency than that of the n-type layer when band tail states or band gap states exist.

The reasons for the phenomena shown in Fig. 4 are complicated. For one thing, in Fig. 4(a), the activation energy in thick samples is larger than that of thinner samples, and the increment of activation energy caused the decline in efficiency, when band tail states and band gap states exist. For another thing, most of the incident light is absorbed in the intrinsic layer if the thickness is sufficient.

The direct band gap absorption is given by

$$\alpha(\hbar\omega) \propto (\hbar\omega - E_g)^{1/2}, \quad (3)$$

where  $\alpha$  is the absorption coefficient,  $\omega$  is the frequency of incident light,  $E_g$  is the energy gap and  $\hbar$  is Planck constant.

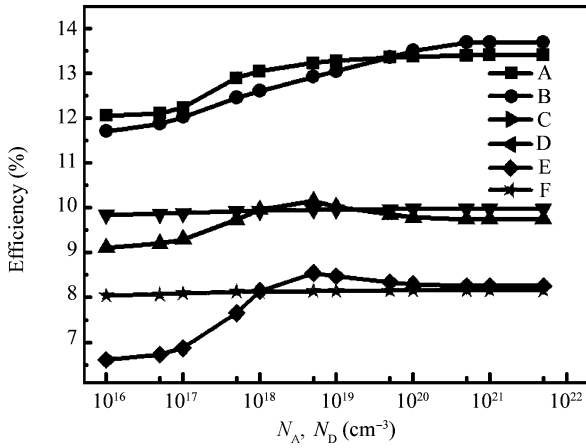


Fig. 5. Impact on efficiency under different conditions of the increment of doping density. A, C and E indicate acceptor densities under the conditions with neither band tail states nor band gap states, band tail states, and both band tail states and band gap states, respectively. B, D and F indicate donor densities under the same conditions with acceptor densities.

The depth of penetration is given by

$$x = \frac{\ln I_0 - \ln[I(x)]}{\alpha}, \tag{4}$$

where  $I_0$  is the initial light intensity, and  $I(x)$  is the light intensity at  $x$ .

$$\lambda_0 = \frac{1.24}{E_g} \text{ (}\mu\text{m)}. \tag{5}$$

where  $I_0$  is the initial light intensity, and  $I(x)$  is the light intensity at  $x$ .

Assume that  $\lambda$  is the wavelength of incident light. If  $\lambda > \lambda_0$ , the incident light will not be absorbed, otherwise, the incident light will be absorbed.

According to the parameters given in Table 1, the threshold wavelengths of a-SiC, a-Si and  $\mu\text{c-Si}$  are 0.681, 0.721 and 0.729  $\mu\text{m}$ , respectively. Based on Eqs. (3) and (4), there is an optimal absorption thickness. If the thickness is less than the optimal absorption thickness, the efficiency will slowly increase. When the thickness reaches the optimal absorption thickness exactly, the efficiency is maximal. Nevertheless, if the thickness exceeds the optimal absorption thickness, the efficiency will decline slightly for extra recombination of electrons and holes caused by long distance transportation.

### 3.3. Doping density

A difference in doping density affects carrier concentration. Figure 5 shows the impact on efficiency of doping density under different conditions ( $N_A$  and  $N_D$  for acceptors and donors, respectively).

From Fig. 5, it can be seen that the donor density has a great impact on the efficiency when band tail states and band gap states exist. Nevertheless, if band tail states and band gap states are neglected, the acceptor density is more important than the donor density to the efficiency.

As the doping density increases, more ionized electrons and holes diffuse to each other so that the built-in electric field between the p-type layer and the n-type layer will be stronger,

hence more photo-induced carriers drift in the strong electric field. Because the defects which result from band tail states and band gap states increase carrier recombination, when band gap states and band tail states are neglected, the loss of photo-induced carriers will be fewer and the photo-induced carriers collected by the cathode and anode are more considerable in the stronger electric field. Nevertheless, when the band tail states and band gap states exist, the Fermi level is pinned in the middle band gap so that the built-in electric field declines. Therefore, the loss of photo-induced carriers that drift in the built-in electric field is much more. The n-type layer acts as a back contact. The incident light is hardly absorbed in this layer. If the doping density exceeds  $10^{20} \text{ cm}^{-3}$ , the material structure and quality will decline and the optical and electrical properties deteriorate, and the balances between the deterioration in material structure and quality and the increase in ionized electrons and holes result in the efficiency nearly holding steady, even though the doping density increases.

## 4. Conclusions

In summary, the interface recombination is crucial to short-circuit current density and efficiency in p-a-SiC:H/i-a-Si:H/n- $\mu\text{c-Si}$  solar cells. The thicknesses of the p-type layer and the intrinsic layer are also vital to the efficiency. The proper thickness of the intrinsic layer is  $\sim 400 \text{ nm}$  when band tail states and band gap states exist. Although the increase in the thickness of the p-type layer has a negative effect on the efficiency, in order to be manufactured to the anode, the thickness of the p-type layer should not be too thin. The acceptor density drastically affects the efficiency when the acceptor density is less than  $10^{19} \text{ cm}^{-3}$ .

Experimentally, the band tail states, band gap states, doping density and interface recombination velocity could be reduced by controlling the growth parameters. By optimizing these growth parameters according to the simulation results of this paper, the efficiency will be enhanced.

## Acknowledgements

The authors gratefully acknowledge Pennsylvania State University, USA, for providing the AMPS-1D simulation package.

## References

- [1] Schönbächler I, Benagli S, Bucher C, et al. Role of i layer deposition parameters on the  $V_{oc}$  and FF of an a-Si:H solar cell deposited by PECVD at 27.13 MHz. *Thin Solid Films*, 2004, 451/452: 250
- [2] Chowdhury A, Mukhopadhyay S, Ray S. Fabrication of thin film nanocrystalline silicon solar cell with low light-induced degradation. *Solar Energy Materials and Solar Cells*, 2009, 93: 597
- [3] Miyazaki K, Fujioka H, Oshima M, et al. A novel a-Si:H solar cell designed by two-dimensional device simulation. *Bulletin of Materials Science*, 1999, 22: 869
- [4] Ulyashin A G, Job R, Scherff M, et al. The influence of the amorphous silicon deposition temperature on the efficiency of the ITO/A-Si:H/C-Si heterojunction (HJ) solar cells and properties of interfaces. *Thin Solid Films*, 2002, 403/404: 35
- [5] Murthy R V R, Dutta V. Underlying reverse current mechanisms in a-Si:H  $p^+ - i - n^+$  solar cell and compact SPICE modeling. *Journal of Non-Crystalline Solids*, 2008, 354: 3780

- [6] Yang J, Yan B, Guha S. Amorphous and nanocrystalline silicon-based multi-junction solar cells. *Thin Solid Films*, 2005, 478: 162
- [7] Saito K, Sano M, Okabe S, et al. Microcrystalline silicon solar cells fabricated by VHF plasma CVD method. *Solar Energy Materials and Solar Cells*, 2005, 86: 565
- [8] Kupich M, Grunsky D, Kumar P, et al. Preparation of microcrystalline single junction and amorphous–microcrystalline tandem silicon solar cells entirely by hot-wire CVD. *Solar Energy Materials and Solar Cells*, 2004, 81: 141
- [9] Hernández-Como N, Morales-Acevedo A. Simulation of heterojunction silicon solar cells with AMPS-1D. *Solar Energy Materials and Solar Cells*, 2009, doi:10.1016/j.solmat.2009.05.021
- [10] Zhang X, Wang X, Xiao H, et al. Simulation of  $\text{In}_{0.65}\text{Ga}_{0.35}\text{N}$  single-junction solar cell. *J Phys D: Appl Phys*, 2007, 40: 7335
- [11] Tripathi S, Venkataramani N, Dusane R O, et al. One-dimensional simulation study of microcrystalline silicon thin films for solar cell and thin film transistor applications using AMPS-1D. *Thin Solid Films*, 2006, 501: 295
- [12] Bouloufa A, Djessas K, Zegadi A. Numerical simulation of  $\text{CuIn}_x\text{Ga}_{1-x}\text{Se}_2$  solar cells by AMPS-1D. *Thin Solid Films*, 2007, 515: 6285
- [13] Demichelis F, Pirri C F, Tresso E. Influence of doping on the structural and optoelectronic properties of amorphous and microcrystalline silicon carbide. *J Appl Phys*, 1992, 72: 1327
- [14] A manual for AMPS-1D. Available on <http://www.cneu.psu.edu/amps/download/>
- [15] Available on [http://www.cneu.psu.edu/amps/ examplesparameters](http://www.cneu.psu.edu/amps/examplesparameters)